Easy access to high-melting sulfurated copolymers and their self-assembling block polymers from phenylisothiocyanate and oxetane

Jenny Stephan,[a] Jorge L. Olmedo-Martínez,[b] Mathias Dimde,[a] Daniel Braatz,[a] Robert Langer,[c] Alejandro J. Müller,[b] Holger Schmalz,[d,e] Alex J. Plajer [d,*]

[a] Institut für Chemie und Biochemie, Freie Universität Berlin, Fabeckstraße 34/36, 14195 Berlin;[b] Department of Polymers and Advanced Materials, Physics, Chemistry and Technology, Faculty of Chemistry, University of the Basque Country UPV/EHU, Paseo Manuel de Lardizabal 3, 20018, Donostia-San Sebastián, Spain; [c] Institut für Chemie, Martin-Luther-Universityät Halle-Wittenberg, Kurt-Mothes-Str. 2, 06120 Halle; [d] Makromolekulare Chemie, Universität Bayreuth, Universitätsstraße 30, 95447 Bayreuth; [e] Bayrischer Polymerinstitut, Universitätsstraße 30, 95447 Bayreuth; *email: alex.plajer@uni-bayreuth.de

Abstract: *Although sulfurated polymers promise unique properties, their controlled synthesis, particularly when it comes to complex and functional architectures, remains challenging. Here, we show that the copolymerization of oxetane and phenyl isothiocyanates quantitatively forms polythioimidocarbonates with narrow molecular weight distributions (M_n = 5–80 kg/mol with $Đ \leq 1.2$; $M_{n,max}$ = 124 kg/mol). Studying their thermal properties through a specially developed self-nucleation procedure, high melting points up to 181 °C are revealed for which π-stacking phenyl substituents and kinetically controlled linkage selectivity are key factors. Tolerance to macro-chain transfer agents and controlled propagation allows the synthesis of double crystalline and amphiphilic block copolymers that enables application in crystallization-driven self-assembly, an unventured territory for sulfurated copolymers.*

Sulfur-containing polymers can exhibit improved semi-crystallinity, recyclability and degradability compared to their all-oxygen-containing counterparts, as well as unique properties, such as high refractive indices as well as the ability to coordinate transition metals rendering them for example useful in optical and sensor applications.[1–11] Here, ring-opening copolymerization (ROCOP) of a strained heterocycle with a heteroallene such as CS_2, COS, and RNCS can provide access to a range of polymer structures that would not be easily attainable otherwise.[12] Much work has focused on the copolymerization of substituted epoxides to produce poly(imido)thiocarbonates using these methods.[13–21] However, these polymers are amorphous if the tacticity of the resulting stereocenter is not controlled. Moving to the unsubstituted case, namely ethylene oxide, does lead to semi-crystalline materials in e.g. the copolymerisation with COS yielding poly(ethylene monothiocarbonate) with a melting point (T_m) of 128°C as now no tacticity control is required, the drawback however is that ethylene oxide is an explosive and highly toxic gas requiring specialised reaction set-ups limiting its' usefulness and applicability in standard research laboratories.[22,23] Transitioning to their unsubstituted liquid four-membered analogue, trimethylene oxide, also known as oxetane (OX), can also lead to unsubstituted polymers that are semi-crystalline. In this context, copolymerization of OX with COS yields poly(trimethylene monothiocarbonate) with a T_m of 128°C.[24,25] Overcoming practical challenges related to the use of gaseous COS, our group and the group of Zhang recently reported linkage-selective CS_2 (a liquid) ROCOP with OX, delivering poly(trimethylene dithiocarbonate) with a lower T_m of 82–89°C.[26,27] However, both copolymerizations result in polymers with a broadened molecular weight distribution ($Đ$ > 1.5) even at molecular weights below M_n = 20 kg/mol. This suggests the occurrence of side reactions alongside propagation, such as chain-end coupling and transesterification processes.[28] Hence moving down the periodic table, while introducing unique material properties, comes at the expense of more side reactions, a problem that extends to many other sulfurated polymer synthesized via ring-opening co- and terpolymerisation.[29–36]

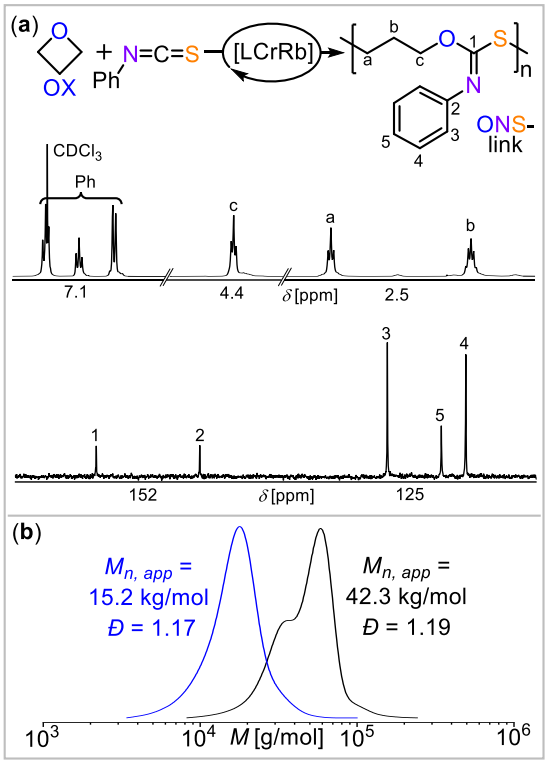

Figure 1: (a) PhNCS/OX ROCOP scheme, ^{1}H and ^{13}C NMR ($CDCl_3$) with assignment corresponding to Table 1 run #1. Overlaid GPC traces of (black) copolymer corresponding to table 1 run #1 and (blue) copolymer obtained from an analogous run in presence of 20 eq. 1,4-benzenedimethanol acting as a bifunctional chain-transfer agent.

These processes reduce the resulting molecular weights and complicate the application of these polymerizations in the synthesis of more complex architectures. Achieving the latter would allow one to rationally combine the properties of established polymers with those of sulfurated ones to obtain new functional materials. The improved semi-crystallinity of sulfurated polymers suggests their usefulness in applications requiring spatially confined

crystallization, such as crystallization-driven self-assembly.[37,38] However only polyethylenesulfide and no sulfurated polyheterocarbonates or esters from RO(CO)P, has been successfully applied in such cases perhaps due to the challenging synthesis of the required amphiphilic block polymers.[39,40] Seeking to address some of these issues, we report here that the copolymerization of PhNCS with OX grants easy access to sulfurated polymers with high melting points and low dispersities as well as their crystallization driven self-assembling block polymers. To achieve the copolymerisation of PhNCS and OX we employed our recently developed heterobimetallic Cr(III)Rb catalyst combining a Cr(III)OAc with a RbOAc complex fragment (LCrRb, see ESI Section S1) which has performed well with other sulfurated monomers.[26,41] PhNCS/OX ROCOP with LCrRb (Table 1 run #1) at a loading of 1 eq. LCrRb**:** 1000 eq. PhNCS: 1000 eq. OX (neat) and 80 ^{o}C for 60 min produces a solid reaction mixture. NMR analysis of the crude mixture reveals 88 % PhNCS and OX consumption and dessymmetrisation of the initially symmetric OX protons into three major CH_2 signals in the ^{1}H NMR spectrum to broad resonances indicating selective polymer formation without any small molecule byproducts.

Table 1: PhNCS/OX copolymerization

Run	Cat.	Cat:PhNCS:OX	*T* [^{o}C]	t [h]	TOF[a]	Polymer Selectivity [%][b]	ONS Selectivity [%][c]	$M_{n,\,app}$ [kg/mol] (*Đ*)[d]
#1	LCrRb	1:1000:1000	80	1	920	>99	95	42.2 (1.19)
#2	LCrNa	1:1000:1000	80	8	180	>99	78	19.4 (1.20)
#3	LCrK	1:1000:1000	80	7	150	>99	87	39.0 (1.16)
#4	LCrRb	1:1000:1000	100	0.3	3300	>99	91	28.0 (1.24)
#5	LCrRb	1:1000:500	80	1	1500	>99	94	31.7 (1.16)
#5	LCrRb	1:2000:2200	80	2	n.d.	>99	95	80.4 (1.20)
#7	LCrRb	1:8000:8200	80	24	n.d.	>99	95	124.0 (1.70)
#8	LCrRb	1:50:50	80	1	n.d	>99	95	4.6 (1.18)
#9[e]	LCrRb	1:1000:1000	80	20	110	89	95	26.0 (1.08)

[a]Turnover frequency (TOF) determined from fitting to initial linear region of the conversion versus time plot obtained by aliquot ^{1}H NMR analysis. [b] Relative integral in the normalised ^{1}H NMR spectrum of resonances from polymer versus small molecule by-products. [c] Relative integral in the normalised ^{1}H NMR spectrum of resonances from ONS repeat units versus OSN repeat units. [d] Apparent number averaged molecular weight determined by GPC (gel permeation chromatography) measurements conducted in THF, using narrow polystyrene standards to calibrate the instrument. [e] Cyclohexyl isothiocyanate was employed in place of PhNCS.

The polymer can be easily isolated from the unconsumed monomers by precipitation from DCM/MeOH followed by drying under vacuum yielding a colourless solid. NMR spectroscopy reveals equimolar incorporation of PhNCS and OX in the isolated polymer and a major heterocarbonate ^{13}C NMR resonance at 157 ppm corresponding to a polymer with –$(CH_2)_3$-O-C(=NPh)-S- links (abbreviated as ONS linkage) in its repeat unit. The imido -C=N- group can also be seen by IR spectroscopy with a characteristic band at $\tilde{\nu}$ = 1630 cm^{-1}. GPC analysis of the isolated polymer reveals a bimodal molecular weight distribution with M_n = 42.2 kg/mol (*Đ* = 1.19) comprising two narrow overlapping distributions where one is centred around ca. half the molecular weight of the other (i.e. 30 and 60 kg/mol). This can be explained by two co-occuring initiation events starting a very controlled PhNCS/OX copolymerisation.[42] IR spectroscopy let us identify aliphatic ester bands ($\tilde{\nu}$ = 1737 cm^{-1}, see ESI Figure S16) from initiation by the acetate coligands of LCrRb whereas end-group analysis by the ^{31}P-test also unambiguously shows the formation of alcohol chain ends (see ESI Figure S17). Combined this suggests the formation of α-OAc,ω-OH functional chains. However as the obtained molecular weight is somewhat lower than the theoretical molecular weight ($M_{n,theo}$ = 170 kg/mol), we infer that chain-transfer reactions with bifunctional protic impurities (typically diols or H_2O) lead to the formation of α,ω-OH telechelic chains which the weight difference of the overlapping distributions supports. Accordingly deliberate addition of bifunctional alcohol chain-transfer reagents (1,4-benzenedimethanol, 20 eq. per LCrRb) to an otherwise analogously conducted copolymerisation leads to a reduction of the obtained molecular weight to M_n = 15.2 kg/mol as well as an apparently monomodal molecular weight distribution with a slightly lower dispersity as now α,ω-OH telechelic chains dominate the sample. Importantly, these results show that propagation during PhNCS/OX ROCOP is very controlled as multimodality arises from different initiation processes.

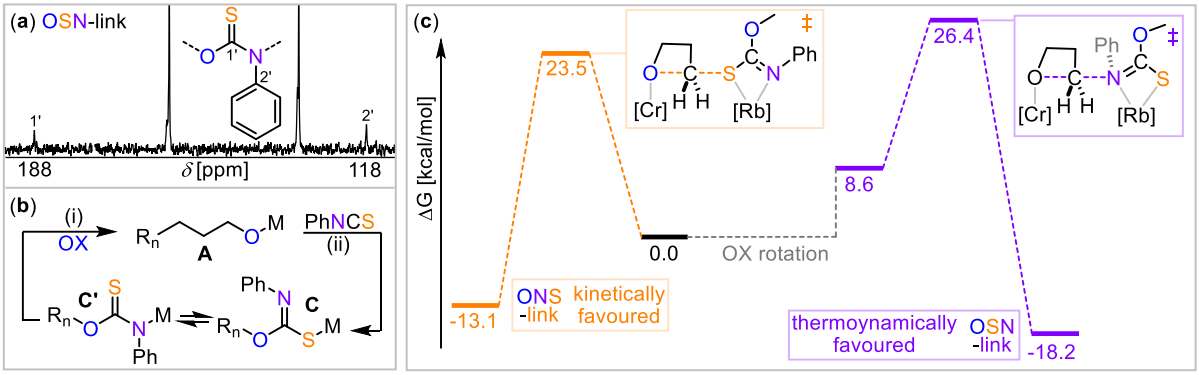

Figure 2: (a) Zoom into the ^{13}C NMR corresponding to table 1 run #3. (b) Hypothetical intermediate speciation leading to ONS and OSN links; M denotes metal catalyst, R_n denotes polymer chain. (c) Computed free energy profile of step (ii) in PTA/OX ROCOP on the ωB97XD/def2-TZVPP level of theory.

With or without added chain-transfer agent, close inspection of the ^1H NMR spectra reveals a second minor set of resonances (5% by integration of the ^1H NMR spectrum). These are associated with a heterocabonate ^{13}C resonance at 188 ppm (**Figure 2(a)**) that can be assigned to thionouretane –$(CH_2)_3$-O-C(=S)-NPh- (OSN) links which effectively represent isomerised ONS groups. Formation of both ONS and OSN links be rationalised by a propagation mechanism as depicted in **Figure 2(b)**.[43] Here catalyst bound alkoxide intermediates **A**, stemming from the OX ring opening in step (i), form an apparent catalyst bound thioimidocarbonates **C** upon PhNCS insertion in step (ii) which react with OX keeping the C=N bond intact to regenerate **A** and form an ONS link. Alternatively, **C** can react from an isomerised structure **C'**, in which the nucleophilic reactivity is centred on the nitrogen rather than the sulfur atom, to form an OSN-link keeping the C=S double intact. To investigate which energetic factors govern the preferential formation of ONS links during propagation we turned to DFT modelling on the ωB97XD/def2-TZVPP level of theory (see ESI Section S8). The assumption of the structure of **C** or **C'** in which the chain end is coordinated in proximity to the incoming OX monomer was chosen in reference to related heteroallene copolymerisations of bimetallic catalysts.[19,44] Here chain end coordination occurs at the alkali metal while OX activation occurs at the adjacent Cr(III) centre on the same side of the catalyst plane. Geometry optimization of the heterocarbonate bound intermediate allowed for the localisation of two discrete minima, in which the heterocarbonate group at the chain-end and the OX either arrange in a coplanar (ΔG = 8.6 kcal/mol) or an almost perpendicular fashion (ΔG = 0.0 kcal/mol). The perpendicular arrangement allows for a S_N2-type nucleophilic attack via the sulfur atom to form an ONS link, which is associated with an activation barrier of $\Delta G^‡$ = 23.5 kcal/mol. The attack via the nitrogen atom to form an OSN link, however, requires rotation of the coordinated OX to allow for a S_N2-type nucleophilic attack of the nitrogen atom with an overall barrier of $\Delta G^‡$ = 26.4 kcal/mol. In terms of insertion thermodynamics, the resulting catalyst bound alkoxide intermediate **A** has a formation energy of -18.1 kcal/mol in the OSN and -13.1 kcal/mol in the ONS case. Combined this shows that the predominantly observed formation of the ONS link occurs on kinetic grounds against what would be the thermodynamically favoured polymer microstructure.

Next, we studied the effects of catalyst choice, monomer loading and reaction temperature on the linkages formed. Changing the alkali metal from Rb (TOF 920 h^{-1}, 95% ONS, run #1) to Na (TOF 180 h^{-1}, 78% ONS, run #2) or K (TOF 150 h^{-1}, 87% ONS, run #3) leads to a substantial decrease of the reaction rate as well as more OSN links demonstrating a clear influence of metal-metal cooperativity on the catalysis. Hence, we continued our studies with LCrRb. Moving from 80 to 100ºC (run #4) leads to an approximate tripling of the rate to a high TOF of 3300 h^{-1} while somewhat reducing molecular weights. Deviating from the 1:1 PhNCS:OX ratio (run #5) maintains rates and selectivity. Decreasing the catalyst loading expectedly increases molecular weights to M_n = 80.4 ($Đ$ = 1.20, run #6) and 124.0 kg/mol ($Đ$ = 1.70, run #7). Conversely at the lowest loading, decreased molecular weights of M_n = 4.6 kDa ($Đ$ = 1.18, run #8) are obtained demonstrating that the methodology lets one access a wide range of weights.

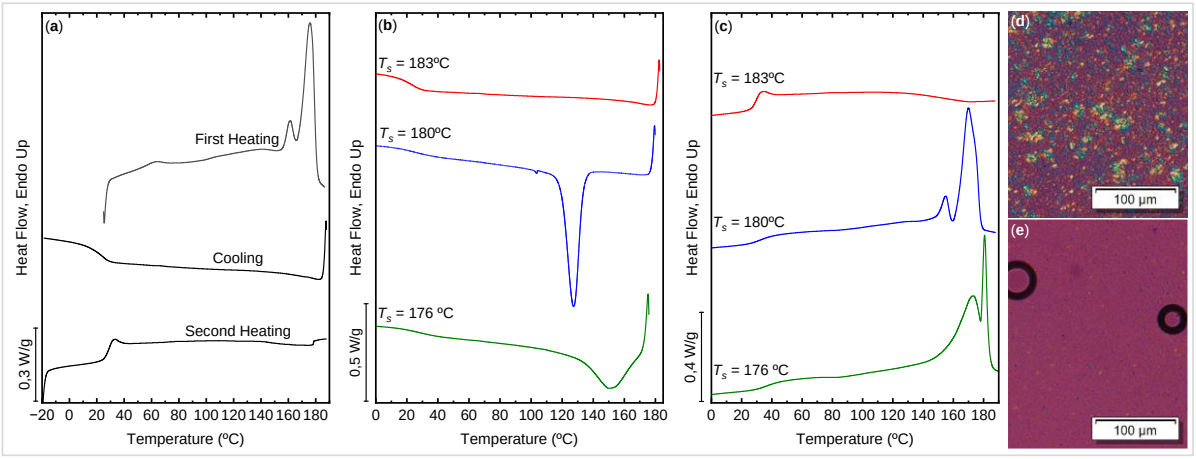

Figure 3: (a) DSC measurements of the polymer sample corresponding to Table 1 run #1. (b) First cooling from selected T_s temperatures and (c) subsequent heating after cooling from T_s. Polarized optical microscopy images of recrystallised polymers corresponding to (d) Table 1 run #1 and (e) Table 1 run #3; round objects surrounded by thick black edges are air bubbles

Next, we studied the thermal properties of the novel poly(thio)imidocarbonate. **Figure 3(a)** shows DSC curves corresponding to the material obtained from Table 1 run #1. The first heating run of the as-synthesized sample shows a complex multimodal endotherm associated with the melting of crystals. The origin of the multiple melting peaks (one broad peak at approximately 140 ºC, followed by two sharp peaks at 165 and 176 ºC) is probably due to melting and reorganization processes during the heating scan performed at 10 ºC/min. The semi-crystalline nature of the polymer could be confirmed by WAXS, showing a degree of crystallinity (X_c) of 52% of the as-synthesized material. Interestingly, the polymer cannot crystallize during cooling at 10 ºC/min, as shown in Figure 3a (see the cooling scan from the melt and the second heating scans that only display glass transitions), and this is also the case for slower cooling rates of 5 and 1 ºC/min. In view of these results, we design a self-nucleation procedure to investigate if self-nuclei could induce crystallization and prove that the reason behind the lack of crystallization from the melt is the slow non-isothermal kinetics of the material. Our procedure could represent a generally applicable tool for the study of sulfurated polymers showing slow crystallisation.[27,41,45] The self-nucleation procedure (SN) procedure employed (see ESI Section S1) consists of utilizing an as-synthesized sample (which is semi-crystalline, as proven in the first heating run of **Figure 3(a)**) and heating it (at 10 ºC/min) to a temperature that we shall denote T_s or self-nucleation temperature. Then, the sample remains at T_s for 3 minutes before it is cooled at 10 ºC/min; hence SN employed differs from traditional SN.[46,47] Depending on T_s, three self-nucleation domains can be defined as follows. The sample will be molten (in the melting *Domain*, or *Domain I*, color code: red in **Figure 3(b)** and **Figure 3(c)**) if T_s is higher than the end of the melting temperature of all crystals present in the sample. In this case, we erased all crystalline thermal history, and the sample is not able to crystallize during cooling from such a high T_s value. The sample will be self-nucleated (*Domain II* or self-nucleation *Domain*, color code: blue in **Figure 3(b)** and **Figure 3(c)**), when T_s is high enough to melt most of the crystals but low enough to leave some self-nuclei. These are regions of the sample where the melt is not isotropic, and the chains retain some of the conformational order they had in the crystals (self-nuclei), or even tiny crystal fragments (i.e., self-seeds). Upon cooling from T_s, the sample will crystallize due to self-nucleation and the second DSC melting trace does not change significantly. Finally, if the T_s is too low, *Domain III* is entered (color code: green in **Figure 3(b)** and **Figure 3(c)**). The sample only partially melts and the unmolten crystal population will anneal during the 3 min at T_s. Upon cooling from T_s, the sample crystallizes at a higher T_c value because of the self-seeding effect of the unmolten crystals, and when the sample is heated for a second time, an additional higher temperature endothermic peak will be generated due to the melting of the annealed crystals.

Figure 3(b) shows cooling scans from the indicated T_s values, while **Figure 3(c)** shows the subsequent heating scans. According to the previous definitions of the self-nucleation domains, 183 ºC is a T_s within *Domain I*, as the sample melted completely, erasing any melt memory in the material and preventing crystallization. If the T_s is lowered to 180 ºC, the sample can be efficiently self-nucleated. This process (i.e., SN) accelerates the non-isothermal crystallization (that comprises both nucleation and growth), and the sample can crystallize with a clear and sharp crystallization exotherm at T_c=127 ºC during cooling from T_s=180 ºC, see **Figure 3(b)**. Hence, this temperature is within *Domain II*. If T_s is further lowered to 176 ºC, the sample enters *Domain III*, as the temperature falls within the melting range of the material, causing partial melting. The sample is able to crystallize self-seeded by the unmolten crystals (**Figure 3(b)**). The unmolten crystals anneal during the 3 min at T_s=176 ºC and melt in the second heating with a sharp peak at 181 ºC. This is one of the highest melting points reported to date for ROCOP copolymers without tacticity control and furthermore lies far above many recently developed sulfur-containing polymers.[3,45,48–52] Similar melting points for these class of copolymers are have only been achieved where molecular weights are limited

(M_n < 20 kg/mol) or not controllable due to e.g. side reactions or zwitterionic propagation pathways.[23,53–55] Polarized Light Optical Microscopy (PLOM) reveals that the crystals formed during cooling were smaller than 0.5 μm and could not be observed by the limiting resolution imposed by the wavelength of visible light. However, after annealing the samples at room temperature for 2 days, crystal superstructures were able to grow, and their microcrystalline texture of small superstructural aggregates was revealed as seen in **Figure 3d**. Furthermore, DSC and PLOM were also performed with the sample from Table 1 run #3, which has a similar M_n but less chain regularity (87% ONS-links). Although the sample is also semi-crystalline (X_c = 53% by WAXS), after SN, it crystallizes and melts at lower temperatures than sample #1 (with 95% ONS links). **Figure 3(e)** shows the polymer with decreased ONS selectivity forms much smaller crystalline aggregates than the one from Table 1 run #1. Intrigued by the semi-crystallinity of the copolymers we wondered whether this is an inherent feature of these OX copolymers comprising the ONS repeat unit. Copolymerising the saturated analogue of PhNCS namely Cyclohexylisothiocyanate with OX (table 1, run #10) leads to copolymerisation at a reduced rate of 110 h^{-1} and polymer selectivity of 89% versus small molecule byproducts. Nevertheless, the copolymer forms in perfect ONS selectivity with a very narrow and monomodal ($Đ$= 1.08) distribution of M_n = 26.0 kg/mol. The material is amorphous by DSC with a T_g=8 ºC which is also apparent from its' translucent nature. This shows that phenyl substitution is vital for semi-crystallinity which we infer to be due to π-stacking as the cyclohexyl substituent has similar size but possess no π-system for such interactions resulting in an amorphous material.

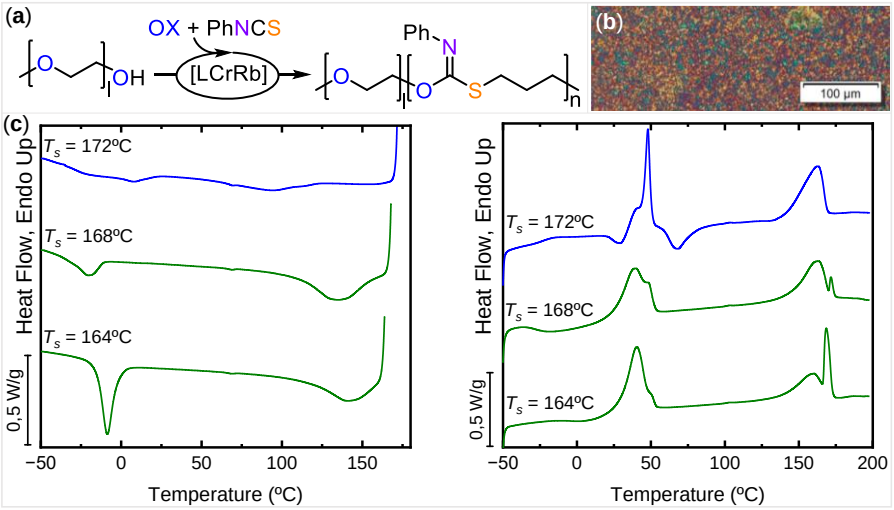

Figure 4: (a) PEG-*b*-(PhNCS-co-OX) synthesised by macro chain transfer strategy. (b) Polarised optical microscopy image of recycrystallised blockpolymer. (c) First cooling from the indicated T_s temperatures and subsequent second heating curve in DSC self-nucleation experiments for the blockpolymer.

Since our results above show that the copolymerisation methodology tolerates chain transfer reactions with alcohols, we hypothesized that the addition of alcohol-terminated polymers acting as macroinitiators could give easy access to functional block polymers. Hence, we added 20 equivalents of polyethyleneglycol-monomethylether (i.e Me-PEG-OH) to a copolymerisation comprising 1 eq. LCrRb: 1000 eq. OX: 1000 eq. PhNCS and obtained a polymer with a final apparent M_n of 8.0 kDa ($Đ$ = 1.01) after precipitation of the crude mixture from DCM/MeOH. Block polymer formation is clearly indicated by the increase in apparent molecular weight compared to the stand-alone Me-PEG-OH macroinitiator. ^{1}H NMR spectroscopy of the precipitated polymer in $CDCl_3$ shows an approximate PEG to PhNCS-co-OX repeat unit ratio of 3:1 by integration. Assuming an Me-PEG length of M_n = 5 kDa (as specified by the supplier) and therefore a DP of 133, this corresponds to a DP of the PhNCS-co-OX of approximately 37. Note that some short acetate-initiated chains due to the co-ligands of the LCrRb catalyst might have formed alongside Me-PEG-OH initiated chains via chain-transfer during the polymerisation and might be present in the sample, although the narrow dispersity indicate that the sample primarily composes of diblock polymer. The non-isothermal standard DSC runs (Figure S 38) show that this diblock copolymer features two distinct crystalline phases for the PEG and PhNCS-co-OX blocks respectively with an overall crystallinity by WAXS of X_c = 49%. Once again, **Figure 4(c)** shows that SN is an effective way to introduce self-nuclei capable of inducing crystallization upon cooling from the appropriate T_s temperature. Furthermore, as the PhNCS-co-OX block crystallizes at higher temperatures from the self-nucleated melt (between 94 and 142 ºC depending on T_s, see Table S4), these crystals can nucleate the PEG block that crystallizes at much lower temperatures (between -21 and 9 ºC). The lower the T_s temperature, the higher the crystallization of both blocks and, in particular, the PEG block, as judged by the latent enthalpies of crystallization reported in Table S 4. Taken together, our results indicate that this diblock copolymer has a clear tendency to self-assemble into distinct crystalline phases. As the constituents have distinct solubilities, i.e., PEG being soluble in water and

alcohols while PhNCS-co-OX is not, we hypothesized that the polymer could be applied in solution self-assembly, which is particularly interesting due to the semi-crystalline but slowly crystallising nature of the PhNCS-co-OX block. This is an unexplored field for sulfurated ROCOP and ROP polymers (except polyethylenesulfide) as the synthesis of the required amphiphiles can be challenging. First, self-assembly in water was investigated via aqueous precipitation. For this purpose, the block polymer was dissolved in 1,4-dioxane and then added dropwise to an aqueous solution under vigorous stirring. Self-assembly is immediately apparent from the formation of a cloudy but homogeneous solution due to the Tyndall effect. Dynamic light scattering (DLS) shows nano-objects with an average size of 126 nm and a dispersity of 0.27. The solution remains stable and the DLS trace remains unchanged over multiple weeks highlighting the stability the aggregates. Cryo transmission electron microscopy (Cryo-TEM) reveals the formation of spherical aggregates. Statistical evalulation of 100 nano objects reveals an average core-diameter of 29.6 ± 0.2 nm (**Figure 5(a)**). Other than these we observe some elongated aggregates with an approximate length of 100-200 nm and a thickness of 10-30 nm although there are too few for a statistical evaluation (ESI Figure S 42). Furthermore a 5-10 nm thick corona presumably corresponding to the water-soluble PEG periphery surrounding a hydrophobic PhNCS-co-OX core can be observed. Assuming a stretched conformation of the PhNCS-co-OX core implies a single repeat unit extends across approximately 0.8 nm based on simple trigonometric considerations and hence 37 repeat units extend across a maximum of 30 nm (Figure S 47). Therefore, the formation of micellar aggregates appears likely as the core diameter of the object observed fall within this range. The elongated aggregates comprise multiples spherical aggregates merging rather than regular cylindrical structures, and this suggest that the cores are amorphous in nature rather than semi-crystalline. We infer that this is due to the slow crystallisation kinetics of PhNCS-co-OX as observed in our DSC studies. We hypothesized that moving to a weaker nonsolvent for the PhNCS-co-OX block in the self-assembly procedure and introducing an additional annealing step might provide sufficient time for core-crystallisation as the insoluble central block is precipitated less abruptly.[56–58] This procedure is efficiently used in crystallization-induced self-assembly (CDSA) of crystalline-coil diblock copolymers, yielding defined core-crystalline micelles in selective solvents for the corona forming blocks. Hence, we repeated the self-assembly procedure outlined above with ethanol in place of water as the nonsolvent for the crystallizable PhNCS-*co*-OX block followed by heating the resulting dispersion at 80°C for 1 day. Formation of a turbid solution due to the Tyndall effect that exhibits no sedimentation of the precipitate over the course of weeks again suggest self-assembly of the block copolymer.

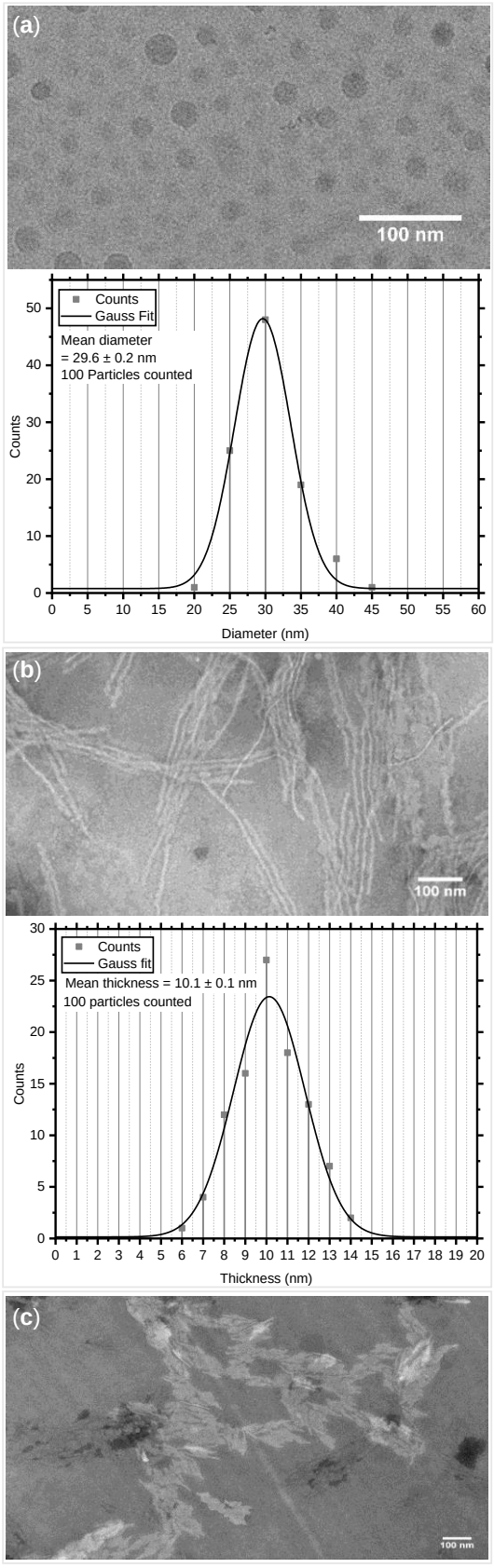

Figure 5: (a) Cryo-TEM image of spherical micellar aggregates obtained via aqueous nanoprecipitation and statistical evaluation of mean diameter. (b) TEM images of cylindrical micelles and statistical evaluation of mean thickness and (c) TEM images of platelets.

TEM reveals the formation of uniform cylindrical micelles which exceed lengths of 500 nm and exhibit a regular shape which stands in contrast to the shorter irregular worm-like aggregates obtained from self-assembly in water. The formation of rather stiff cylindrical micelles is a typical feature of CDSA and, thus, points to crystallization as driving force for self-assembly in ethanol. They cylinders possess narrowly distributed thicknesses between 6 and 14 nm with a statistical average of 10.1 ± 0.1 nm. Such a thickness points towards a folding of the PhNCS-co-OX chains within the cores. Heating of the analogous sample for another 3 days results in a different morphology as apparent from a shift in the DLS trace from an average diameter of 170 to 770 nm. TEM reveals the fusion of the cylindrical micelles obtained after 1 day to platelet-like structures although these structures are less uniform than the cylindrical aggregates from before. Similar platelets can also be obtained by sonification of the bulk material followed by annealing although further investigation of ROCOP polymers in crystallisation driven self-assembly are required.

Conclusions

In conclusion, we have established the copolymerization of oxetane with phenyl isothiocyanate as a practical method to obtain sulfurated copolymers. The method can delivers materials at high molecular weights that exhibit some of the highest melting points in the field. To study their crystallization behaviour, we have developed a new self-nucleation procedure that revealed kinetically governed linkage selectivity, as well as phenyl substitution, to be key in maximizing crystallinity. Demonstrating the utility of the new polymerization, we have prepared an amphiphilic and double-crystalline block polymer for which the crystallization of one block seeds the crystallization of the other. Because of the crystallization kinetics, nanostructures with different morphologies, including amorphous (spherical and worm-like aggregates) and semi-crystalline cores (cylindrical micelles and platelets), can be obtained depending on the self-assembly conditions in the solution. Owing to the degradability and recyclability benefits that sulfurated polymers exhibit, PhNCS-co-OX could represent an alternative to established polymers in engineering plastics, optical or optoelectronic applications.

Acknowledgements

The VCI is acknowledged for a Liebig Fellowship. We would like to acknowledge the assistance of the Core Facility BioSupraMol.

Conflict of Interest

There are no conflicts of interest.

Bibliography

(1) Yue, T.-J.; Ren, W.-M.; Lu, X.-B. Copolymerization Involving Sulfur-Containing Monomers. *Chem. Rev.* **2023**, *123, 24, 14038–14083* https://doi.org/10.1021/acs.chemrev.3c00437.

(2) Jia, J.; Liu, J.; Wang, Z.-Q.; Liu, T.; Yan, P.; Gong, X.-Q.; Zhao, C.; Chen, L.; Miao, C.; Zhao, W.; Cai, S. (Diana); Wang, X.-C.; Cooper, A. I.; Wu, X.; Hasell, T.; Quan, Z.-J. Photoinduced Inverse Vulcanization. *Nat. Chem.* **2022**, *14* (11), 1249–1257. https://doi.org/10.1038/s41557-022-01049-1.

(3) Wang, Y.; Li, M.; Chen, J.; Tao, Y.; Wang, X. O-to-S Substitution Enables Dovetailing Conflicting Cyclizability, Polymerizability, and Recyclability: Dithiolactone vs. Dilactone. *Angew. Chem. Int. Ed.* **2021**, *60* (41), 22547–22553. https://doi.org/10.1002/anie.202109767.

(4) Yue, T.-J.; Ren, B.-H.; Zhang, W.-J.; Lu, X.-B.; Ren, W.-M.; Darensbourg, D. J. Randomly Distributed Sulfur Atoms in the Main Chains of CO2-Based Polycarbonates: Enhanced Optical Properties. *Angew. Chem. Int. Ed.* **2021**, *60* (8), 4315–4321. https://doi.org/10.1002/anie.202012565.

(5) Zhang, J.; Bai, T.; Liu, W.; Li, M.; Zang, Q.; Ye, C.; Sun, J. Z.; Shi, Y.; Ling, J.; Qin, A.; Tang, B. Z. All-Organic Polymeric Materials with High Refractive Index and Excellent Transparency. *Nat Commun* **2023**, *14* (1), 3524. https://doi.org/10.1038/s41467-023-39125-w.

(6) Su, Y.-L.; Yue, L.; Tran, H.; Xu, M.; Engler, A.; Ramprasad, R.; Qi, H. J.; Gutekunst, W. R. Chemically Recyclable Polymer System Based on Nucleophilic Aromatic Ring-Opening Polymerization. *J. Am. Chem. Soc.* **2023***, 145, 25, 13950–13956*. https://doi.org/10.1021/jacs.3c03455.

(7) Xia, Y.; Yue, X.; Sun, Y.; Zhang, C.; Zhang, X. Chemically Recyclable Polyethylene-like Sulfur-Containing Plastics from Sustainable Feedstocks. *Angew. Chem. Int. Ed.* **2023**, *62* (13), e202219251. https://doi.org/10.1002/anie.202219251.

(8) Sobotta, F. H.; Kuchenbrod, M. T.; Gruschwitz, F. V.; Festag, G.; Bellstedt, P.; Hoeppener, S.; Brendel, J. C. Tuneable Time Delay in the Burst Release from Oxidation-Sensitive Polymersomes Made by PISA. *Angew. Chem. Int. Ed.* **2021**, *60* (46), 24716–24723. https://doi.org/10.1002/anie.202108928.

(9) Zhang, J.; Zang, Q.; Yang, F.; Zhang, H.; Sun, J. Z.; Tang, B. Z. Sulfur Conversion to Multifunctional Poly(O-Thiocarbamate)s through Multicomponent Polymerizations of Sulfur, Diols, and Diisocyanides. *J. Am. Chem. Soc.* **2021**, *143* (10), 3944–3950. https://doi.org/10.1021/jacs.1c00243.

(10) Peng, J.; Tian, T.; Xu, S.; Hu, R.; Tang, B. Z. Base-Assisted Polymerizations of Elemental Sulfur and Alkynones for Temperature-Controlled Synthesis of Polythiophenes or Poly(1,4-Dithiin)s. *J. Am. Chem. Soc.* **2023**, *145* (51), 28204–28215. https://doi.org/10.1021/jacs.3c10954.

(11) Tian, T.; Hu, R.; Tang, B. Z. Room Temperature One-Step Conversion from Elemental Sulfur to Functional Polythioureas through Catalyst-Free Multicomponent Polymerizations. *J. Am. Chem. Soc.* **2018**, *140* (19), 6156–6163. https://doi.org/10.1021/jacs.8b02886.

(12) Plajer, A. J.; Williams, C. K. Heterocycle/Heteroallene Ring-Opening Copolymerization: Selective Catalysis Delivering Alternating Copolymers. *Angew. Chem. Int. Ed.* **2022**, *61* (1), e202104495. https://doi.org/10.1002/anie.202104495.

(13) Zhu, X.-F.; Xie, R.; Yang, G.-W.; Lu, X.-Y.; Wu, G.-P. Precisely Alternating Copolymerization of Episulfides and Isothiocyanates: A Practical Route to Construct Sulfur-Rich Polymers. *ACS Macro Lett.* **2021**, *10* (1), 135–140. https://doi.org/10.1021/acsmacrolett.0c00831.

(14) Zhu, X.-F.; Yang, G.-W.; Xie, R.; Wu, G.-P. One-Pot Construction of Sulfur-Rich Thermoplastic Elastomers Enabled by Metal-Free Self-Switchable Catalysis and Air-Assisted Coupling. *Angew. Chem. Int. Ed.* **2022**, *61* (7), e202115189. https://doi.org/10.1002/anie.202115189.
(15) Zhu, X.-F.; Lu, X.-Y.; Xu, C.-K.; Fang, Y.-B.; Yang, G.-W.; Li, W.; Wang, J.; Wu, G.-P. Alternating Copolymerization of Epoxides and Isothiocyanates to Diverse Functional Polythioimidocarbonates and Related Block Polymers. *Chin. J. Chem.* **2023**, *41* (23), 3311–3318. https://doi.org/10.1002/cjoc.202300266.
(16) Rupf, S.; Pröhm, P.; Plajer, A. J. Lithium Achieves Sequence Selective Ring-Opening Terpolymerisation (ROTERP) of Ternary Monomer Mixtures. *Chem. Sci.* **2022**, *13* (21), 6355–6365. https://doi.org/10.1039/D2SC01776H.
(17) Silbernagl, D.; Sturm, H.; Plajer, A. J. Thioanhydride/Isothiocyanate/Epoxide Ring-Opening Terpolymerisation: Sequence Selective Enchainment of Monomer Mixtures and Switchable Catalysis. *Polym. Chem.* **2022**, *13* (27), 3981–3985. https://doi.org/10.1039/D2PY00629D.
(18) Deglmann, P.; Machleit, S.; Gallizioli, C.; M. Rupf, S.; J. Plajer, A. Lithium Catalysed Sequence Selective Ring Opening Terpolymerisation: A Mechanistic Study. *Cat. Sci. Tech.* **2023**, *13* (10), 2937–2945. https://doi.org/10.1039/D3CY00301A.
(19) Stephan, J.; Stühler, M. R.; Rupf, S. M.; Neale, S.; Plajer, A. J. Mechanistic Mapping of (CS2/CO2)/Epoxide Copolymerization Catalysis Leads to Terpolymers with Improved Degradability. *Cell Rep. Phys. Sci.* **2023**, 101510. https://doi.org/10.1016/j.xcrp.2023.101510.
(20) Geng, X.; Liu, Z.; Zhang, C.; Zhang, X. Toward Stereo- and Sequence-Defined Block Copolymers via a Three-Site Organocatalyst. *Macromolecules* **2023**, *56* (12), 4649–4657. https://doi.org/10.1021/acs.macromol.3c00623.
(21) Zhang, C.-J.; Zhu, T.-C.; Cao, X.-H.; Hong, X.; Zhang, X.-H. Poly(Thioether)s from Closed-System One-Pot Reaction of Carbonyl Sulfide and Epoxides by Organic Bases. *J. Am. Chem. Soc.* **2019**, *141* (13), 5490–5496. https://doi.org/10.1021/jacs.9b00544.
(22) Ren, W.-M.; Yue, T.-J.; Li, M.-R.; Wan, Z.-Q.; Lu, X.-B. Crystalline and Elastomeric Poly(Monothiocarbonate)s Prepared from Copolymerization of COS and Achiral Epoxide. *Macromolecules* **2017**, *50* (1), 63–68. https://doi.org/10.1021/acs.macromol.6b02089.
(23) Yang, J.-L.; Wang, Y.; Cao, X.-H.; Zhang, C.-J.; Chen, Z.; Zhang, X.-H. Enabling Oxygen–Sulfur Exchange Reaction to Produce Semicrystalline Copolymers from Carbon Disulfide and Ethylene Oxide. *Macromol. Rapid Commun.* **2021**, *42* (3), 2000472. https://doi.org/10.1002/marc.202000472.
(24) Wu, H.-L.; Yang, J.-L.; Luo, M.; Wang, R.-Y.; Xu, J.-T.; Du, B.-Y.; Zhang, X.-H.; Darensbourg, D. J. Poly(Trimethylene Monothiocarbonate) from the Alternating Copolymerization of COS and Oxetane: A Semicrystalline Copolymer. *Macromolecules* **2016**, *49* (23), 8863–8868. https://doi.org/10.1021/acs.macromol.6b02285.
(25) Cao, X.; Wang, H.; Yang, J.; Wang, R.; Hong, X.; Zhang, X.; Xu, J.; Wang, H. Sulfur-Substitution-Enhanced Crystallization and Crystal Structure of Poly(Trimethylene Monothiocarbonate). *Chin. Chem. Lett.* **2022**, *33* (2), 1021–1024. https://doi.org/10.1016/j.cclet.2021.07.014.
(26) Fornacon-Wood, C.; Manjunatha, B. R.; Stühler, M. R.; Gallizioli, C.; Müller, C.; Pröhm, P.; Plajer, A. J. Precise Cooperative Sulfur Placement Leads to Semi-Crystallinity and Selective Depolymerisability in CS2/Oxetane Copolymers. *Nat. Commun.* **2023**, *14* (1), 4525. https://doi.org/10.1038/s41467-023-39951-y.
(27) Feng, G.; Feng, X.; Liu, X.; Guo, W.; Zhang, C.; Zhang, X. Metal-Free Alternating Copolymerization of CS2 and Oxetane. *Macromolecules* **2023**, *56, 17, 6798–6805*. https://doi.org/10.1021/acs.macromol.3c01300.
(28) Xu, J.; Zhang, P.; Yuan, Y.; Hadjichristidis, N. Elucidation of the Alternating Copolymerization Mechanism of Epoxides or Aziridines with Cyclic Anhydrides in the Presence of Halide Salts. *Angew. Chem. Int. Ed.* **2023**, *62, e2022188* https://doi.org/10.1002/anie.202218891.
(29) Jurrat, M.; Pointer-Gleadhill, B. J.; Ball, L. T.; Chapman, A.; Adriaenssens, L. Polyurethanes and Polyallophanates via Sequence-Selective Copolymerization of Epoxides and Isocyanates. *J. Am. Chem. Soc.* **2020**, *142* (18), 8136–8141. https://doi.org/10.1021/jacs.0c03520.
(30) Sengoden, M.; Bhat, G. A.; Darensbourg, D. J. Explorations into the Sustainable Synthesis of Cyclic and Polymeric Carbonates and Thiocarbonates from Eugenol-Derived Monomers and Their Reactions with CO2, COS, or CS2. *Green Chem.* **2022**, *24* (6), 2535–2541. https://doi.org/10.1039/D2GC00327A.
(31) Clark, E. F.; Kociok-Köhn, G.; Davidson, M. G.; Buchard, A. Polymers from Sugars and Isothiocyanates: Ring-Opening Copolymerization of a D-Xylose Anhydrosugar Oxetane. *Polym. Chem.* **2023**, 14, 2838–2847.
(32) McGuire, T. M.; Buchard, A. Polymers from Sugars and CS2: Ring Opening Copolymerisation of a D-Xylose Anhydrosugar Oxetane. *Polym. Chem.* **2021**, *12* (29), 4253–4261. https://doi.org/10.1039/D1PY00753J.
(33) Wang, L.-Y.; Gu, G.-G.; Yue, T.-J.; Ren, W.-M.; Lu, X.-B. Semiaromatic Poly(Thioester) from the Copolymerization of Phthalic Thioanhydride and Epoxide: Synthesis, Structure, and Properties. *Macromolecules* **2019**, *52* (6), 2439–2445. https://doi.org/10.1021/acs.macromol.9b00073.
(34) Luyer, S. L.; Quienne, B.; Bouzaid, M.; Guégan, P.; Caillol, S.; Illy, N. Bio-Based Poly(Ester-Alt-Thioether)s Synthesized by Organo-Catalyzed Ring-Opening Copolymerizations of Eugenol-Based Epoxides and N-Acetyl Homocysteine Thiolactone. *Green Chem.* **2021**, *23* (19), 7743–7750. https://doi.org/10.1039/D1GC02138A.
(35) Song, L.; Liu, M.; You, D.; Wei, W.; Xiong, H. Alternating Chain Growth Copolymerization of Isothiocyanates and Epoxides. *Macromolecules* **2021**, *54* (22), 10529–10536. https://doi.org/10.1021/acs.macromol.1c01561.
(36) Tran, D. K.; Braaksma, A. N.; Andras, A. M.; Boopathi, S. K.; Darensbourg, D. J.; Wooley, K. L. Structural Metamorphoses of D-Xylose Oxetane- and Carbonyl Sulfide-Based Polymers In Situ during Ring-Opening Copolymerizations. *J. Am. Chem. Soc.* **2023**, *145, 33, 18560–18567.* https://doi.org/10.1021/jacs.3c05529.
(37) MacFarlane, L.; Zhao, C.; Cai, J.; Qiu, H.; Manners, I. Emerging Applications for Living Crystallization-Driven Self-Assembly. *Chem. Sci.* **2021**, *12* (13), 4661–4682. https://doi.org/10.1039/D0SC06878K.
(38) Pearce, A. K.; Wilks, T. R.; Arno, M. C.; O'Reilly, R. K. Synthesis and Applications of Anisotropic Nanoparticles with Precisely Defined Dimensions. *Nat Rev Chem* **2021**, *5* (1), 21–45. https://doi.org/10.1038/s41570-020-00232-7.
(39) Sevgen, E.; Dolejsi, M.; Nealey, P. F.; Hubbell, J. A.; de Pablo, J. J. Nanocrystalline Oligo(Ethylene Sulfide)-b-Poly(Ethylene Glycol) Micelles: Structure and Stability. *Macromolecules* **2018**, *51* (23),

9538–9546. https://doi.org/10.1021/acs.macromol.8b01812.
(40) Brubaker, C. E.; Velluto, D.; Demurtas, D.; Phelps, E. A.; Hubbell, J. A. Crystalline Oligo(Ethylene Sulfide) Domains Define Highly Stable Supramolecular Block Copolymer Assemblies. *ACS Nano* **2015**, *9* (7), 6872–6881. https://doi.org/10.1021/acsnano.5b02937.
(41) Fornacon-Wood, C.; Stühler, M. R.; Gallizioli, C.; Manjunatha, B. R.; Wachtendorf, V.; Schartel, B.; Plajer, A. J. Precise Construction of Weather-Sensitive Poly(Ester-Alt-Thioesters) from Phthalic Thioanhydride and Oxetane. *Chem. Commun.* **2023***, 59, 11353-11356*.
(42) R. Stühler, M.; Gallizioli, C.; M. Rupf, S.; J. Plajer, A. Ring-Opening Terpolymerisation of Phthalic Thioanhydride with Carbon Dioxide and Epoxides. *Polym. Chem.* **2023**, *14* (42), 4848–4855. https://doi.org/10.1039/D3PY01022H.
(43) Yang, J.; Zhen, L.; Jiang, L. Synthesis of N,N-Disubstituted Thiocarbamates from Thiocarbamoyl Fluorides with Alcohols/Phenols/Thiophenols/Thioalcohols Through Copper Catalysis. *ChemistrySelect* **2019**, *4* (20), 6177–6180. https://doi.org/10.1002/slct.201901294.
(44) Deacy, A. C.; Phanopoulos, A.; Lindeboom, W.; Buchard, A.; Williams, C. K. Insights into the Mechanism of Carbon Dioxide and Propylene Oxide Ring-Opening Copolymerization Using a Co(III)/K(I) Heterodinuclear Catalyst. *J. Am. Chem. Soc.* **2022**, *144* (39), 17929–17938. https://doi.org/10.1021/jacs.2c06921.
(45) Wang, Y.; Zhu, Y.; Lv, W.; Wang, X.; Tao, Y. Tough While Recyclable Plastics Enabled by Monothiodilactone Monomers. *J. Am. Chem. Soc.* **2023***, 145, 3, 1877–1885*. https://doi.org/10.1021/jacs.2c11502.
(46) Michell, R. M.; Mugica, A.; Zubitur, M.; Müller, A. J. Self-Nucleation of Crystalline Phases Within Homopolymers, Polymer Blends, Copolymers, and Nanocomposites. In *Polymer Crystallization I: From Chain Microstructure to Processing*; Auriemma, F., Alfonso, G. C., de Rosa, C., Eds.; Advances in Polymer Science; Springer International Publishing: Cham, 2017; pp 215–256. https://doi.org/10.1007/12_2015_327.
(47) Sangroniz, L.; Cavallo, D.; Müller, A. J. Self-Nucleation Effects on Polymer Crystallization. *Macromolecules* **2020**, *53* (12), 4581–4604. https://doi.org/10.1021/acs.macromol.0c00223.
(48) Zhu, Y.; Li, M.; Wang, Y.; Wang, X.; Tao, Y. Performance-Advantaged Stereoregular Recyclable Plastics Enabled by Aluminum-Catalytic Ring-Opening Polymerization of Dithiolactone. *Angew. Chem. Int. Ed.* **2023**, *62* (24), e202302898. https://doi.org/10.1002/anie.202302898.
(49) Xia, Y.; Yuan, P.; Zhang, Y.; Sun, Y.; Hong, M. Converting Non-Strained γ-Valerolactone and Derivatives into Sustainable Polythioesters via Isomerization-Driven Cationic Ring-Opening Polymerization of Thionolactone Intermediate. *Angew. Chem. Int. Ed.* **2023**, *62* (14), e202217812. https://doi.org/10.1002/anie.202217812.
(50) Yuan, P.; Sun, Y.; Xu, X.; Luo, Y.; Hong, M. Towards High-Performance Sustainable Polymers via Isomerization-Driven Irreversible Ring-Opening Polymerization of Five-Membered Thionolactones. *Nat. Chem.* **2022**, *14* (3), 294–303. https://doi.org/10.1038/s41557-021-00817-9.
(51) Sehn, T.; Huber, B.; Fanelli, J.; Mutlu, H. Straightforward Synthesis of Aliphatic Polydithiocarbonates from Commercially Available Starting Materials. *Polym. Chem.* **2022**, *13* (42), 5965–5973. https://doi.org/10.1039/D2PY00990K.
(52) Zhu, Y.; Tao, Y. Stereoselective Ring-Opening Polymerization of S-Carboxyanhydrides Using Salen Aluminum Catalysts: A Route to High-Isotactic Functionalized Polythioesters. *Angew. Chem. Int. Ed.* ***2024****,* e202317305. https://doi.org/10.1002/anie.202317305.
(53) Soga, K.; Hattori, I.; Sato, M.; Ikeda, S. Copolymerization of Carbon Disulfide and N-(β-Cyanoethyl)Ethylenimine. *J. Polym. Sci.: Polym. Chem.* **1979**, *17* (1), 215–224. https://doi.org/10.1002/pol.1979.170170121.
(54) Tan, D.; Hu, X.; Cao, Z.; Luo, M.; Darensbourg, D. J. Zwitterionic Alternating Polymerization to Generate Semicrystalline and Recyclable Cyclic Polythiourethanes. *ACS Macro Lett.* **2020**, *9* (6), 866–871. https://doi.org/10.1021/acsmacrolett.0c00302.
(55) Yokota, H.; Kondo, M. Alternating Copolymerization of Carbonyl Sulfide with Aziridines. *J. Polym. Sci.: Polym. Chem.* **1971**, *9* (1), 13–25. https://doi.org/10.1002/pol.1971.150090102.
(56) Inam, M.; Cambridge, G.; Pitto-Barry, A.; Laker, Z. P. L.; Wilson, N. R.; Mathers, R. T.; Dove, A. P.; O'Reilly, R. K. 1D vs. 2D Shape Selectivity in the Crystallization-Driven Self-Assembly of Polylactide Block Copolymers. *Chem. Sci.* **2017**, *8* (6), 4223–4230. https://doi.org/10.1039/C7SC00641A.
(57) Kwon, Y.; Kim, K. T. Crystallization-Driven Self-Assembly of Block Copolymers Having Monodisperse Poly(Lactic Acid)s with Defined Stereochemical Sequences. *Macromolecules* **2021**, *54* (22), 10487–10498. https://doi.org/10.1021/acs.macromol.1c01825.
(58) Jiang, J.; Nikbin, E.; Hicks, G.; Song, S.; Liu, Y.; Wong, E. C. N.; Manners, I.; Howe, J. Y.; Winnik, M. A. Polyferrocenylsilane Block Copolymer Spherulites in Dilute Solution. *J. Am. Chem. Soc.* **2023**, *145* (2), 1247–1261. https://doi.org/10.1021/jacs.2c11119.